Research Article Wiley Online Library ELECTROANALYSIS

doi.org/10.1002/elan.202100563

A Stable Porphyrin Functionalized Graphite Electrode Used at the Oxygen Evolution Reaction Potential

Gianlorenzo Bussetti,*[a] Roberto Bernasconi,[b] Claudia Filoni,[a] Luca Magagnin,[b] Alberto Bossi,[c] Franco Ciccacci,[a] and Lamberto Duò[a]

Abstract: Many researches have been devoted to rechargeable power generators that can store (but also release) energy. This availability is ensured through (*e.g.*) the oxygen evolution reaction (OER). However, (i) large values of the overpotentials and (ii) a progressive detriment of the anode (graphite) electrode limit the ultimate device. In view of enhancing the electrode performances, graphite was protected by following different strategies, which oblige to follow precise preparation protocols. Here, we prove that a thin layer of free-base porphyrin molecules is able to protect the underneath graphite electrode from detriment even if many (about 100) electrochemical cycles are performed.

Keywords: graphite intercalation · porphyrin protective layer · EC-AFM · X-ray photoelectron spectroscopy (XPS) · SEM

1 Introduction

The rising global demand of energy requires new and economic solutions [1]. In fuel cells, the main problems are the role of the oxygen evolution reaction (OER) overpotential and the detriment of some electrodes such as graphite [1–3].

Generally speaking, polymers are usually adopted to protect carbon-based materials even if they are unstable and can produce unwanted contamination in the electrolytes. Another strategy foresees the growth of metal oxides shields (*e.g.*, TiO_2 nanowires arrays). However, this protection can be significantly affected by surface defects, which make the shields vulnerable. An alternative strategy to solve the latter problem foresees the protection of the graphite electrode by means of thin and ultrathin coatings; the growth of such films enables for preserving the graphite transport characteristics and reduces the amount of material required for the electrode protection [4,5].

In former studies, we observed that even a single over layer of free-base porphyrin (H_2TPP), which is able to reversibly exchange charges with the surface during the oxidation of the main tetrapyrrole ring, preserves the underneath graphite from detriment, when the electrode is immersed inside an acid electrolyte solution [5]. In fact, if a freshly prepared highly oriented pyrolytic graphite (HOPG) crystal is exploited as an electrode in acid solution (this choice is almost obliged to perform a microscopic investigation), the basal plane undergoes a serious detriment when the OER is reached at a proper positive electrochemical (EC) potential [6]. Solvated ions can intercalate inside the graphite lamellar crystal structure and, as well as on the uppermost graphite layer, oxygen, carbon mono-oxide and carbon di-oxide evolve within the underneath layers [7]. However, being the graphite layers (*i.e.*, graphene sheets) not permeable to gases, the latter are able to swell the graphite basal plane and create blisters on the HOPG surface [6,7]. Blisters generally show a lateral size of hundreds of nanometers up to the micrometer length scale, while their height is in the range of some tens of nanometers. Blister evolution cannot be avoided because they immediately appear when the electrode EC potential is reduced with respect to the intercalation/OER one [6]. In addition, if the HOPG electrode is kept above the OER potential value, HOPG undergoes a serious carbon dissolution [8].

On the other hand, organic (namely, porphyrin) layers present interesting electrochemical properties [9,10], which can be easily tuned by modifying the chemical structure of the molecules [11]. Indeed, their redox behavior can be tailored by modifying the structure of the aromatic ring or by introducing a transition metal ion in the central tetradentate region of the porphyrin ring [12]. This second option has been widely investigated in the

[a] G. Bussetti, C. Filoni, F. Ciccacci, L. Duò
Department of Physics, Politecnico di Milano, Italy
E-mail: gianlorenzo.bussetti@polimi.it
[b] R. Bernasconi, L. Magagnin
Department of Chemistry, Materials and Chemical Engineering "G. Natta", Politecnico di Milano, Italy
[c] A. Bossi
Istituto di Scienze e Tecnologie Chimiche "G. Natta" del Consiglio Nazionale delle Ricerche (CNR-SCITEC), and SmartMatLab Centre, Milano, Italy

Supporting information for this article is available on the WWW under https://doi.org/10.1002/elan.202100563

literature and the electrochemical properties of the so called metalloporphyrins are well-known [13]. Furthermore, porphyrins are characterized by a high electromagnetic radiation absorption, which allows photoexcitation and direct manipulation of the energetic levels of the molecule. Thanks to their peculiar properties, they find application in photovoltaics, energy conversion field [14], photodynamic therapy [15], catalysis [16] or spintronics [17].

In a quite recent publication, Singh and co-workers exploited H_2TPP molecules as corrosion inhibitors for steel electrodes [18]. Porphyrin films can be obtained by drop-casting [19], Langmuir-Blodgett technique [20] or by sublimation in vacuum [21]. Following the latter strategy, well-ordered, continuous, and ultra-thin films can be observed on inorganic substrates, such as graphite [22]. In addition, free-base porphyrins can interact with acid species through the N atoms of the pyrrole rings [23]. Porphyrins oxidation further promotes efficient electron transfer to the graphite electrode [24,25] and, considering the well-ordered and continuous array that can be obtained over a HOPG surface [22], the possibility of anion intercalation inside the buried electrode could become negligible.

In this work, we thus compare two graphite electrodes, one directly exposed to an acid electrolyte, the second one previously protected by a porphyrin thin film. Our results will prove that (i) the porphyrin/graphite system can work as electrode and (ii) the organic protection is stable after a hundred of cyclic-voltammetries (CVs), which reach the OER potential. We believe that our findings can help the research on graphite electrode protection for application in fuel cells.

2 Experimental Methods

A HOPG substrate, purchased from Optigraph, was used during the experiments. The specimen $(25\times25\times1)$ mm^3 was exfoliated in air by an adhesive tape before each experiment. The prepared HOPG was used for the organic deposition (see below) and transferred to the different experimental set-ups handling carefully the substrate but without any particular protocol.

For the preparation of the porphyrin film, a H_2TPP powder (Merck) was placed in a crucible inside an organic molecular beam epitaxy chamber (Kenosistec KE-500 OMBE, base pressure in low 10^{-5} Torr). A quartz microbalance (QMC), placed in proximity of the sample, can monitor the molecular flux from the Knudsen cell. The QMC can work even during the preparation of the sample. When a stable flux (0.4–0.5 Å/s) was obtained at about 360 °C, the HOPG substrate (always kept at room temperature) was placed in front of the crucible at a distance of about 30 cm. The exposure time was decided in view of obtaining a thin porphyrin film having a nominal thickness of 20 nm. This substrate burial is required to avoid domain boundaries in the organic film through which acid ions can percolate inside, so circumventing the deposited protective layer.

HOPG is exploited as the working electrode (WE) inside a three-electrode cell. The WE area was about 0.2 cm^2. A Pt wire is inserted inside the cell as the counter electrode (CE). Despite not being a real reference electrode, a second Pt wire is inserted inside the cell to work as a quasi-reference (Pt-QRef) [26]. The possibility of using only a wire for the EC potential reference is suitable for *in-situ* measurements considering that the EC cell is designed for the coupling with a microscope. The Pt-QRef is stable in acid electrolytes within few millivolts and shows a shift of 0.74 V with respect to the standard hydrogen electrode (SHE). The EC-cell (made in Teflon) can be filled with 2 ml of 1 mM H_2SO_4 electrolyte. The latter was de-aereated by bubbling Ar inside a funnel for several hours.

Both HOPG and H_2TPP/HOPG samples were also tested as macroelectrodes performing CVs in 200 ml of either 1 mM H_2SO_4, 0.5 M H_2SO_4 or 1 M KOH solutions. In the case of 1 mM H_2SO_4, a Pt wire was used as quasi-reference,again. For 0.5 M H_2SO_4 and 1 M KOH solutions, on the contrary, a standard saturated KCl silver-silver chloride (SSC) reference electrode was employed. In both cases, a platinized titanium net was used as CE. A constant area of 0.64 cm^2 was selected on the samples. No stirring was employed, and the scan rate was fixed at 25 mV/s. Solutions were de-aerated prior to electrochemical testing by bubbling pure nitrogen inside a funnel for 3 hours.

A commercial Keysight 5500 atomic force microscopy (AFM) was employed for the *in-situ* and real-time characterization of the electrode surface. The scanner head can be immersed inside the EC cell and the acquisition can be coupled with the CV, which is driven by a potentiostat. The images were collected in non-contact mode in view of preserving possible sulfate adsorbates. The tips (Nano Sensors, $k=30$ N/m) were made of silicon and shown a resonance frequency in air of about 300 kHz. The latter is reduced at about 1/3 when the cantilever oscillates inside the electrolyte. The cantilever had an Al coating to enhance the reflection of the laser beam focused on it. Aluminum coatings degrade when the AFM scanner is immersed inside the sulfuric electrolyte and the intensity of the reflection beam is partially reduced. This occurrence, which does not inquinate or change the quality of the electrolyte, does not preclude the acquisition of good images during the scan.

Concerning the X-ray photoelectron spectroscopy (XPS) analysis, the samples were inserted in the vacuum system after flushing the surface by air. Samples were mounted on the substrate holder and transferred to the fast entry chamber. When the pressure reached 5×10^{-7} Torr in the fast entry, the sample were transferred to the ultra-high vacuum system (base pressure of 1×10^{-10} Torr). The XPS analysis was performed with an unmonochromatized Mg Kα source (photon energy

1253.6 eV) operated at a power of 200 W. The photoemission system consists of a 150 mm hemispherical analyzer working at a pass energy of 20 eV. The combined full width at half maximum resolution of the photon source and the spectrometer was below 1 eV.

Finally, scanning electron microscopy (SEM) images were acquired at 15 kV by a portable TM 4000-II (Hitachi) microscope.

3 Results and Discussion

Figure 1a shows the first CV profile of the unprotected HOPG electrode. A peak at around 1.2 V is observed. This is traditionally interpreted as the intercalation stage occurring immediately after the OER (0.92 V) [8]. The cathodic (negative) feature (about 1.0 V) is usually related to the de-intercalation process. The presence of a positive and negative signal in the Faradaic current gives a quasi-reversible character to the overall intercalation process [7]. Panels *b* and *c* report two subsequent CVs acquired after the first one (panel *a*). It is clear that the overall Faradaic current has increased its intensity and the intercalation feature is now more evident and placed at a lower EC potential value (1.15 V) because the graphite electrode presents more damages caused during the first CV. If the electrode surface shows more defects, the latter represent preferential paths for the anion intercalation. In addition, the general surface-to-volume ratio is increased due to the enhancement of the surface roughness.

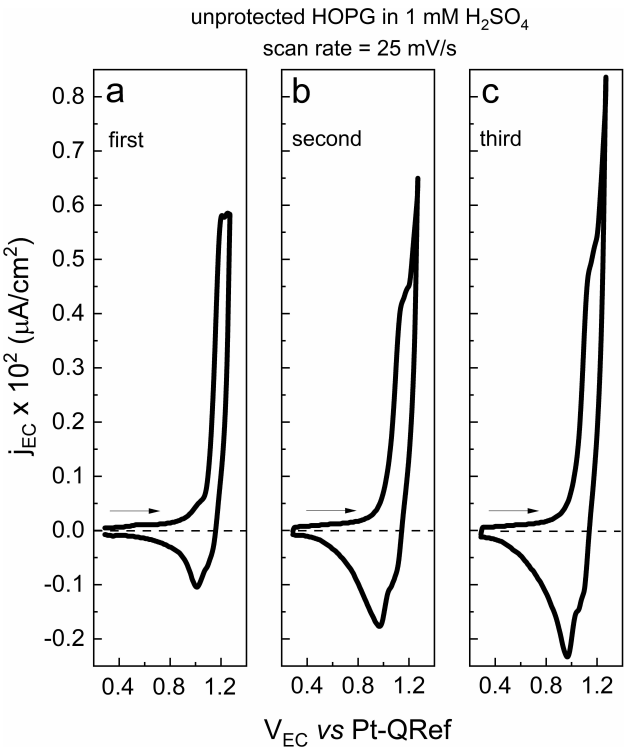

Fig. 1. subsequent CVs acquired onto a freshly prepared HOPG electrode. The arrows indicate the direction of the EC potential sweep.

The changes in the morphological behavior of the electrode surface can be observed by the *in-situ* analysis performed through AFM and reported in Figure 2.

In panel *a*, we show the electrode surface topography acquired when the EC potential is set at a 0.3 V *vs* Pt-QRef, where no Faradaic currents flow through the sample. The traditional graphite stepped surface is clearly observed at this EC potential value. This means that the electrode surface is preserved from any detriment. The morphological evolution of the graphite basal plane as a function of the EC potential, swept during the first CV, is reported in panel *b*. The white dashed lines enclose the topographic interval where the CV is run. The morphology suddenly changes as soon as the cathodic peak (white dotted line, see also Figure 1*a*) is reached, in very good agreement with previous results reported and discussed by the authors [6]. Now, the basal plane is characterized by blisters and a general detriment of the electrode surface is found. Subsequent CVs (please, refer to panels *c* and *d*) only show that new blisters can appear while other vanish probably because of a deflation of the swelled area.

In Figure 3, we report the phase-contrast images related to those shown in Figure 2. Despite the topography proves that graphite steps are well visible and stable at 0.3 V, the phase-contrast image (panel *a*) shows some roundish objects that are placed on or next to the steps [29]. Such features are due to some acid depositions preferentially adsorbed close to defect areas, and they have not any preferential direction (roundish shape). These deposits or precipitates can appear because each AFM frame is acquired within some minutes to avoid image artefacts caused by a fast tip scan inside the liquid electrolyte. Comparing with the other panels of Figure 3, we observe that such roundish deposits are present even after the first CV and they can change their position. Blisters can grow close to such features but, in general, there is not a superposition between them.

Figure 4 shows, on a relative larger scale (150 μm), the surface of the H_2TPP protected HOPG electrode as acquired *ex-situ* by a SEM. The image proves the coating high quality due to the porphyrins film: all the explored areas seem to be homogeneously covered and tiniest graphite steps are not visible. Only high steps (see the figure) are clearly visible.

When immersed inside the acid electrolyte, the H_2TPP/HOPG CV is significantly affected by the presence of the organic film, as reported in Figure 5. Here, a peak appears at 0.85 V during the anodic potential sweep while, during the cathodic one, no significant negative features are detected (in comparison with, *e.g.*, the CV reported in Figure 6 of ref. 30). In that work, the high intensity cathodic feature is interpreted in terms of sulphate species deintercalation that here seems to be avoided. The positive peak is related to the oxidation process occurring at the porphyrin tetrapyrrole ring [23].

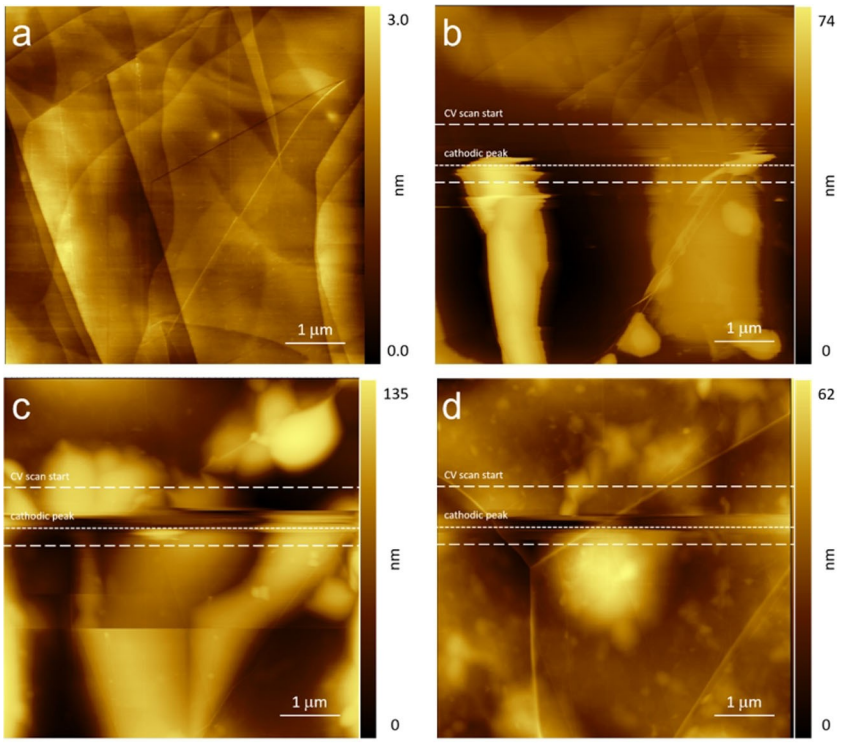

Fig. 2. topographic analysis of the HOPG electrode immersed inside 1 mM H_2SO_4 electrolyte. The white dashed lines (see, CV scan start) enclose the region where the CV is acquired. The dotted lines (cathodic peak) highlight when the de-intercalation peak is reached.

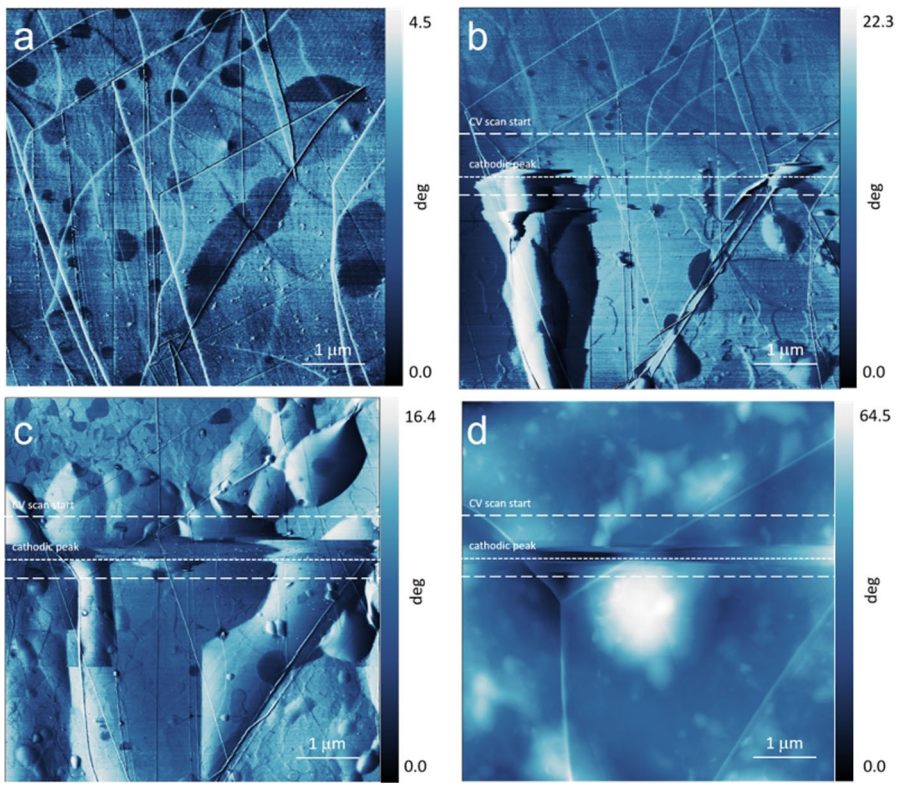

Fig. 3. phase-contrast analysis of the HOPG electrode immersed inside 1 mM H_2SO_4 electrolyte. The white dashed lines (see, CV scan start) enclose the region where the CV is acquired. The dotted lines (cathodic peak) highlight when the de-intercalation peak is reached.

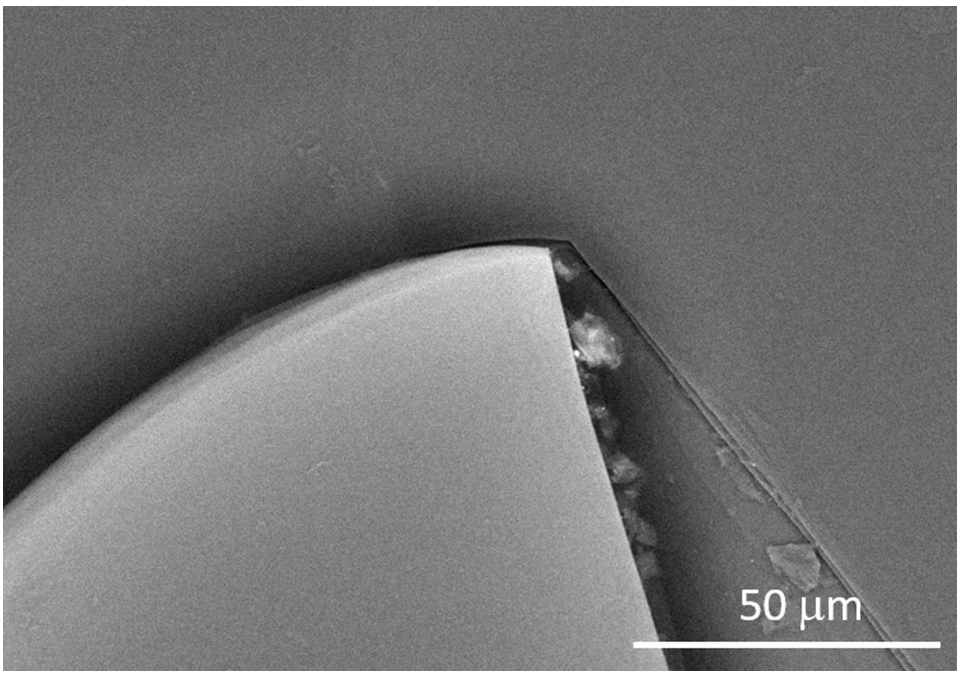

Fig. 4. SEM image of the protected graphite electrode before the immersion inside the electrolyte.

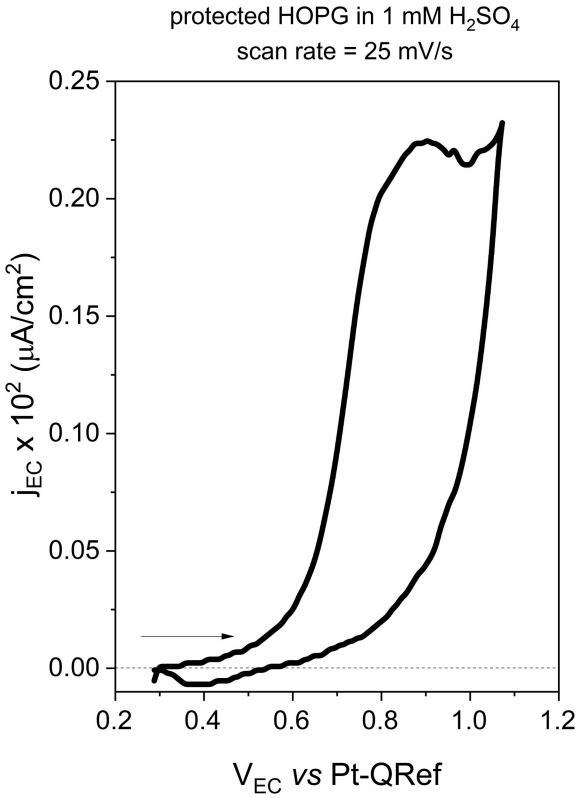

Fig. 5. an electrochemical characterization (CV) performed onto a protected graphite electrode covered by free base porphyrins.

In addition, we note that the overpotential for the OER is reduced if compared with the CV of the unprotected graphite electrode reported in Figure 1*a* (0.5 V and 0.92 V, respectively, to obtain the same Faradaic current density, i. e., 2 µA/cm^2).

An inspection of the pristine protected electrode surface by AFM highlights the presence of porphyrin crystals [32], as reported in Figure 6a. These crystals were the topic of another investigation, where we proved their stability inside sulfuric solutions [31]. However, it is possible to completely dissolve these crystals by electrochemistry [32]. In fact, after few CVs, the electrode morphology is significantly changed: nanocrystals are not visible any more, while a residual film seems to homogenously cover the electrode surface (see panels *c* and *d*). This film is stable even when a hundred of CVs are acquired (see panels *e* and *f*). During these CVs (see Figure 7), which are extended between −1.4 V and 1.6 V, allowing porphyrins to undergo both oxidation and reduction processes, it is not possible to observe any characteristic graphite intercalation or deintercalation feature. This means that solvated anions are not able to circumvent the residual 2D porphyrin film and the buried graphite basal plane is thus protected. Only at the end of these numerous amounts of CVs, we observe a lowering of the porphyrin features (arrows in the highlighted regions of Figure 7). Probably, this represents a definitive detriment of the porphyrin 2D layer that starts to have holes (see panel *c* in Figure 6) where solvated anions can reach the buried HOPG, intercalate and swell its basal plane.

Finally, the exploited WE is investigated *ex-situ* by SEM to observe any other morphological feature on a wider length scale (about 150 µm). In Figure 8, we report the acquired image, where graphite steps clearly appear again and some residuals (probably porphyrins with

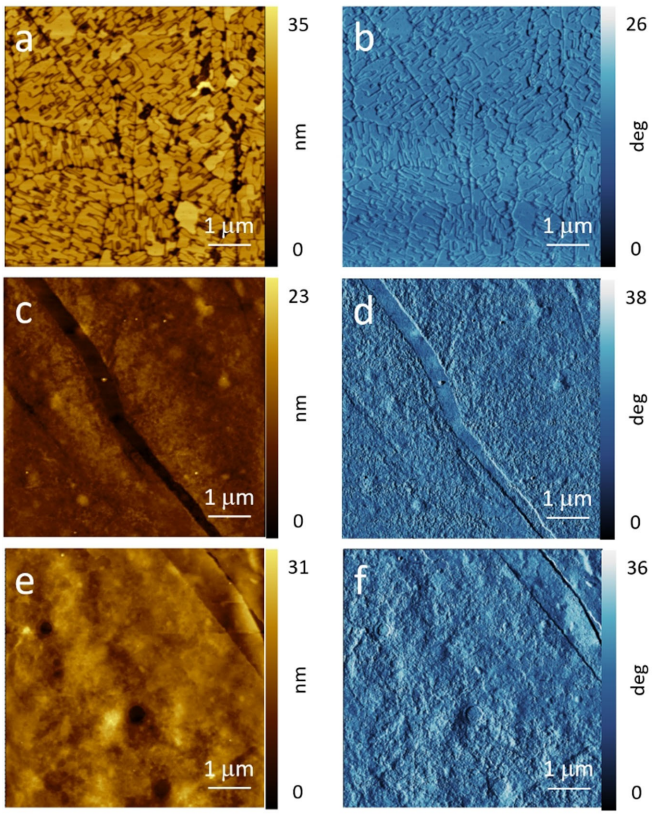

Fig. 6. topographic (*a, c, e*) and phase-contrast (*b, d, f*) analysis of the H_2TPP protected HOPG electrode immersed inside 1 mM H_2SO_4 electrolyte. Panels *a* and *b* refer to the as-prepared sample immersed inside the electrolyte at 0.3 V. Panels *c* and *d* are acquired after about 10 CVs, when the porphyrin crystals are completely dissolved while panels *e* and *f* are collected after a hundred of CVs.

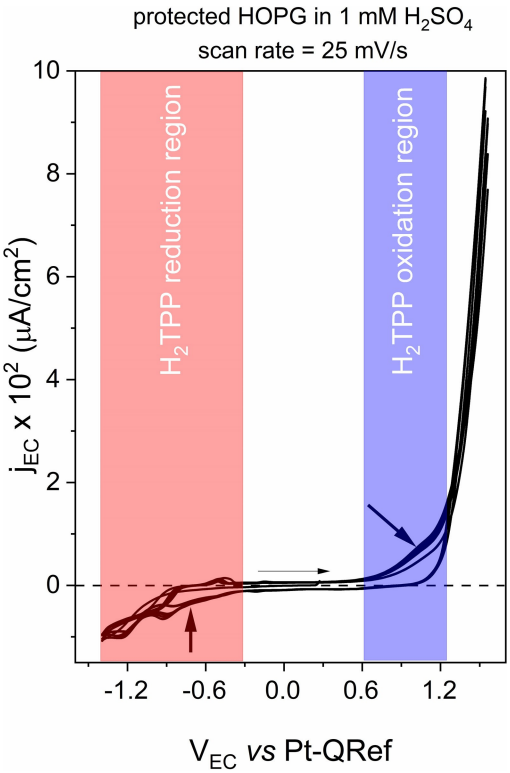

Fig. 7. subsequent CVs (about 100) acquired onto a protected HOPG electrode. We report only part of the whole collected data for a better readability. The arrows in the reduction and oxidation regions show a lowering of the porphyrin features that occurs close the end of our cycles.

sulfate anions and other compounds obtained during the CVs), are randomly distributed on the electrode surface.

Porphyrin functionalized HOPG was also investigated as macro electrode in 0.5 M H_2SO_4 and 1 M KOH. The first electrolyte allowed determining the effect of an increase in sulfuric acid concentrations with respect to the 1 mM case, while the latter was selected since it represents a typical choice for the evaluation of OER performances for electrocatalysts [33,34].

However, before using the 0.5 M H_2SO_4 and 1 M KOH electrolytes, the previously EC characterization performed onto the porphyrin protected graphite electrode (see Figure 5) was repeated on the macro electrode to verify the data correspondence. Figure 9a depicts the obtained results (using a comparable potential range between 0.3 and 1.2 V *vs* Pt). The behavior observed in Figure 5 is almost perfectly reproduced in panel *a*, with an anodic peak visible at around 0.85 V during the anodic potential sweep and no negative features visible in the cathodic branch. In the second cycle, the anodic peak at 0.85 V almost disappeared due to the practically complete oxidation of the porphyrin layer present on the surface of the electrode.

CV cycling was repeated as well on the macro electrode, yielding the result visible in panel *b*. In this case, the scan range was extended to 0.3–1.5 V *vs* Pt.

In analogy with the behavior observed in Figure 7, the Faradaic current density increases in the first cycles of the experiment. Then, all the voltammograms tended to superimpose at high cycle numbers. This is reasonably indicative of a progressive stabilization of the electrode behavior as the residual porphyrin film formed.

After verifying the compliance of the behavior observed on the macro electrode to the measures previously carried out, porphyrin functionalized HOPG was tested in 0.5 M sulfuric acid. This solution was characterized by a much more aggressive environment with respect to the 1 mM electrolyte, with visible consequences on the stability of the residual porphyrin film [33]. Initially, the behavior of the electrode was investigated in the same potential range as the 1 mM H_2SO_4 case (0.3–1.5 V *vs* SSC, as reported in Figure 10a). 50 cycles were performed in this range.

The electrode showed a diametrically opposed behavior with respect to the 1 mM sulfuric acid case. Faradaic current values tend to lower by increasing cycles, indicating a reasonable progressive damaging of the porphyrin

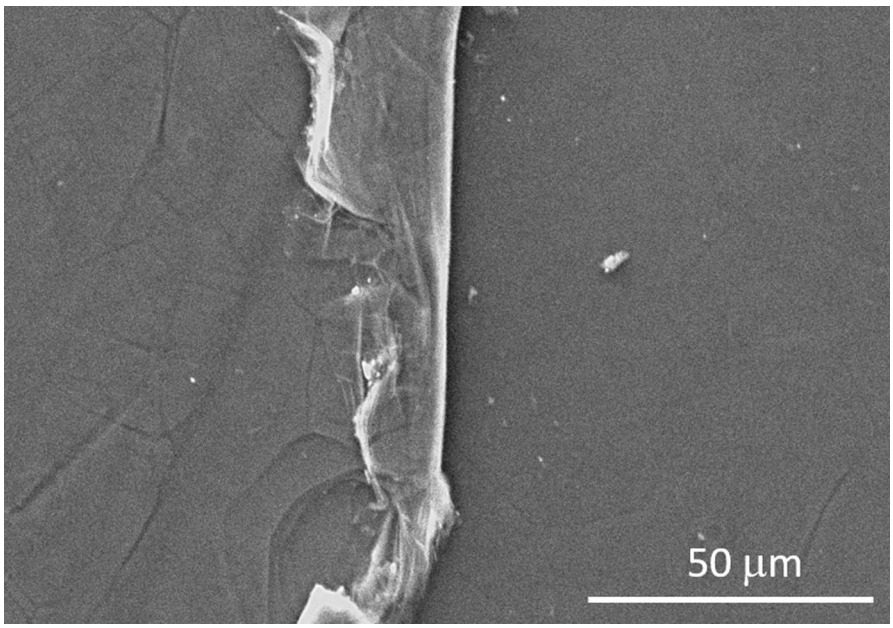

Fig. 8. SEM image of the protected graphite electrode after the immersion inside the electrolyte and the electrochemical treatment.

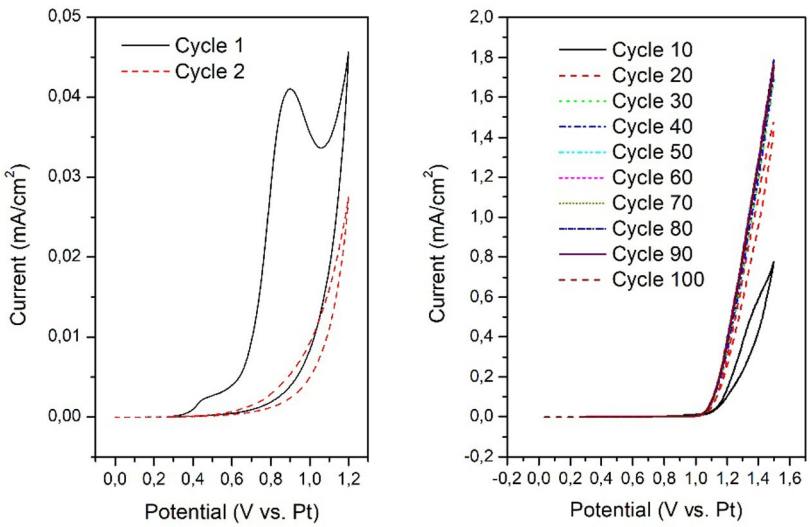

Fig. 9. electrochemical characterization performed on a protected graphite macro electrode covered by free-base porphyrins in 1 mM H_2SO_4 (a); 100 CV cycles performed on a protected graphite macro electrode covered by free-base porphyrins in 1 mM H_2SO_4 (b).

layer and a disappearance of the electrocatalytic effect [33].

The effect of potential scan range was verified by increasing the range, after the first 50 cycles, to 0.6–1.8 V *vs* SSC. The result obtained is visible in panel *b*. The electrode withstood the first cycles at the new potential range without showing any appreciable sign of intercalation. Then, starting from the 70th cycle, graphite showed evident signs of intercalation as a progressive growth of the cathodic peak visible at 1.65 V *vs* SSC. The attribution of that peak to graphite intercalation was ensured by performing a CV on uncoated HOPG. Apparently, the strongly acidic condition induced by the high concentration of sulfuric acid (pH = 0.3) badly affected the stability of the porphyrin layer. However, the latter was surprisingly able to withstand 50 cycles in the 0.3–1.5 V *vs* SSC range and 10 in the 0.6–1.8 V *vs* SSC range without showing appreciable signs of intercalation.

Contrarily to what observed in the 1 mM H_2SO_4 electrolyte, the overpotential for OER progressively increased with respect to the CV of the unprotected graphite HOPG (for example, at a current density of 200 µA/cm^2, it was equal to 1.73 V vs. SSC at the 100th cycle, which is higher than the value observed for the unprotected HOPG, 1.66 V vs. SSC). This effect con-

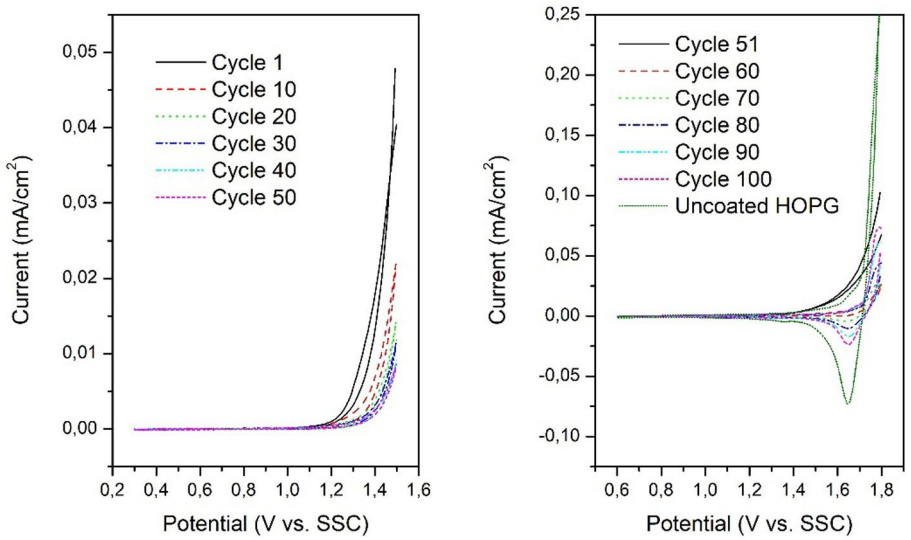

Fig. 10. 50 CV cycles performed between 0.3 and 1.5 V *vs* SSC on a protected graphite macro electrode covered by free base porphyrin in 0.5 M H_2SO_4 (a); 50 CV cycles performed between 0.6 and 1.8 V *vs* SSC on a protected graphite macro electrode covered by free base porphyrin in 0.5 M H_2SO_4 (b).

stitutes another evidence that HOPG progressively lost its protective layer and anion intercalation started.

Finally, a porphyrin bearing macro electrode was tested in 1 M KOH. Like for 0.5 M sulfuric acid, the 0.3–1.5 V *vs* SSC potential range was initially used. The result obtained is shown in Figure 11a.

In analogy with what observed in the 1 mM sulfuric acid electrolyte, also in 1 M KOH currents progressively increased by increasing the number of cycles. This indicates a progressive stabilization of the electrode as the residual porphyrin layer formed. To verify the effect of potential range, the latter was increased to 0.6–1.8 V *vs* SCC after the first 50 cycles. In this context, the electrode showed a relatively stable behavior, with no apparent signs of porphyrin layer damaging. OER overpotential was significantly lowered by the presence of the porphyrin layer (for example, at a current density of 2 mA/cm^2, it was equal to 0.95 V vs. SSC at the 100th cycle, which is

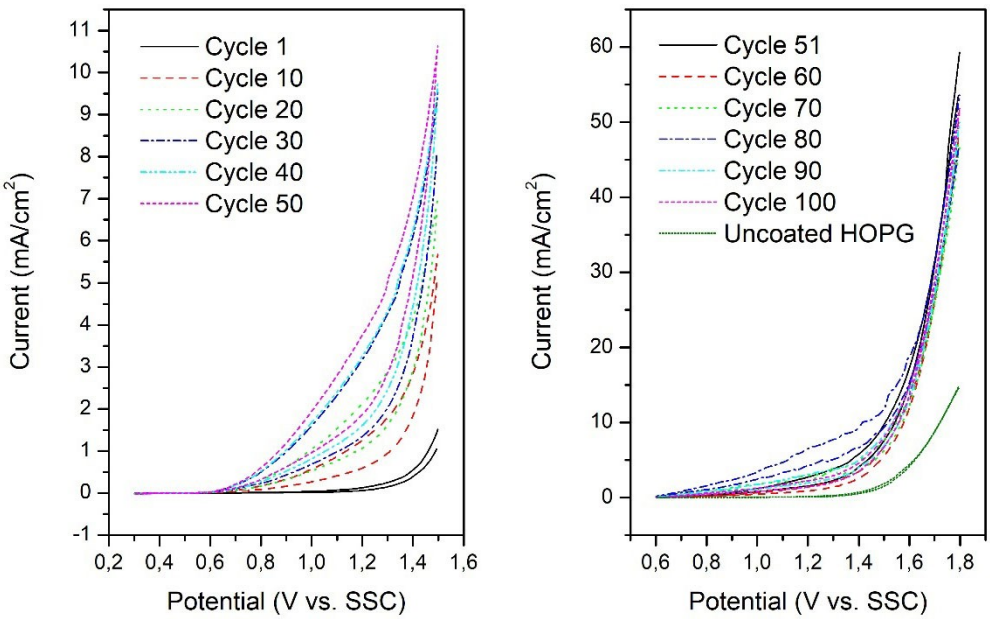

Fig. 11. 50 CV cycles performed between 0.3 and 1.5 V *vs* SSC on a protected graphite macro electrode covered by free-base porphyrins in 1 M KOH (a); 50 CV cycles performed between 0.6 and 1.8 V *vs* SSC on a protected graphite macro electrode covered by free-base porphyrins in 1 M KOH (b).

considerably lower than the value observed for the unprotected HOPG, 1.44 V vs. SSC). To obtain the same Faradaic current density, i.e., 10 mA/cm^2, porphyrin protected HOPG required 1.51 V *vs* SCC, whereas unprotected HOPG required 1.72 V *vs* SCC. This effect is clearly indicative of a catalytic behavior towards OER in alkaline environment.

It is worth discussing in detail the promising result obtained in the case of OER in 1 M KOH. In general, porphyrins present active sites able to catalyze a wide range of multielectron EC reactions. They are active as electrocatalysts toward hydrogen evolution reaction (HER) [35] and oxygen reduction reaction (ORR) [36]. In the case of OER, however, stability issues can affect their performances. Porphyrins, in the specific case metallo-porphyrin monolayers, have been reported to have a limited stability toward OER in alkaline conditions [37], since positive potentials induce a rapid decomposition of the organic backbone of the molecules. However, these considerations have been done on Au electrodes, which present a limited interaction with the porphyrin itself. In the case of carbonaceous electrodes, the interaction is much stronger, resulting into conjugation of the moiety with the material (which can be graphite [36], glassy carbon [35] or even nanotubes [38]). Such conjugation depends on the type of porphyrin used or on its substituents [22], it stabilizes the monolayer in contact with the substrate and it can explain the behavior observed in Figure 11. In fact, the same coupling that allows the formation of the residual film may realistically stabilize the porphyrin itself, allowing stable cycling at high potentials in 1 M KOH.

4 Conclusions

Graphite electrodes play an important role in fuel cells even if some limitations are observed, such as the measured overpotentials in the OER and a general detriment of the electrode surface quality. Our research has recently focused its attention on the second topic. In particular, we observe that free-base porphyrin molecules, when deposited onto the HOPG surface by evaporation in vacuum, create a homogeneous film that is able to protect the buried graphite surface from solvated ion intercalation. The latter mechanism can swell the graphite basal plane and induces a general detriment of the electrode. In this work, we prove that intercalation is precluded for many (about a hundred) CVs if the HOPG is protected by porphyrins. The original organic film morphology (3D crystals) changes after the very first cycles reaching a condition where no further evolutions are observed (2D porphyrin film). We believe that these findings can encourage a systematic investigation on porphyrin thin films as promising coatings for electrodes in acid environments.

Acknowledgments

The authors are grateful to B. Shirzadi, I. Majumdar and A. Calloni (Politecnico di Milano), F. Renzi and A. Spaziani (Quantum Design Europe) for useful discussions. Open Access Funding provided by Politecnico di Milano within the CRUI-CARE Agreement.

Data Availability Statement

Data available on request from the authors.

References

[1] J. Wang, H.-X. Zhong, Y.-L. Qin, X.-B. Zhang, *Angew. Chem.* **2013**, *125*, 5356.
[2] M.-X. Qiao, Y. Zhang, L.-F. Zhai, M. Sun, *Chem. Eng. J.* **2018**, *344*, 410.
[3] M. S. Jagadeesh, G. Bussetti, A. Calloni, R. Yivlialin, L. Brambilla, A. Accogli, E. Gibertini, D. Alliata, C. Goletti, F. Ciccacci, L. Magagnin, C. Castiglioni, L. Duò, *J. Phys. Chem.* **2019**, *C 123*, 1790.
[4] B. Haghighi, H. Hamidi, L. Gorton, *Sens. Actuators B* **2010**, *147*, 270.
[5] R. Yivlialin, G. Bussetti, M. Penconi, A. Bossi, F. Ciccacci, M. Finazzi, L. Duò, *ACS Appl. Mater. Interfaces* **2017**, *9*, 4100.
[6] R. Yivlialin, L. Brambilla, A. Accogli, E. Gibertini, M. Tommasini, C. Goletti, M. Leone, L. Duò, L. Magagnin, C. Castiglioni, G. Bussetti, *Appl. Surf. Sci.* **2020**, *504*, 144440.
[7] K. W. Hathcock, J. C. Brumfield, C. A. Goss, E. A. Irene, R. W. Murray, *Anal. Chem.* **1995**, *67*, 2201.
[8] R. Yivlialin, G. Bussetti, L. Magagnin, F. Ciccacci, L. Duò, *Phys. Chem. Chem. Phys.* **2017**, *19*, 13855.
[9] D. G. Davis, Electrochemistry of porphyrins-The porphyrins (2012).
[10] H. H. Inhoffen, P. Jäger, R. Mählhop, C. Mengler, *EurJOC* **1967**, *704–1*, 188.
[11] K. M. Kadish, E. V. Caemelbecke, *J. Solid State Electrochem.* **2003**, *7*, 254.
[12] X. Lu, S. Devaramani, Electrochemical Investigation of Porphyrin and Its Derivatives at Various Interfaces (2017).
[13] R. Guilard, K. M. Kadish, *Chem. Rev.* **1988**, *88*, 1121.
[14] J. M. Park, J. H. Lee, W. Jang, *Coord. Chem. Rev.* **2020**, *407*, 213157.
[15] T. W. Liu, El. Huynh, T. D. MacDonald, G. Zheng, *Cancer Ther.* **2014**, *229*.
[16] T. He, C. Zhang, G. Will, A. Du, *Catal. Today* **2020**, *351*, 113.
[17] D. M. Lopes, J. C. Araujo-Chaves, L. R. Menezes, I. L. Nantes-Cardoso, *Intech Open* (2020).
[18] A. Singh, Y. Lin, M. A. Quraishi, L. O. Olasunkanmi, O. E. Fayemi, Y. Sasikumar, B. Ramaganthan, I. Bahadur, I. B. Obot, A. S. Adekunle, M. M. Kabanda, E. E. Ebenso, *Molecules* **2015**, *20*, 15122.
[19] R. Paolesse, S. Nardis, D. Monti, M. Stefanelli, C. Di Natale, *Chem. Rev.* **2017**, *117*, 2517.
[20] G. Giancane, L. Valli, *Adv. Colloid Interface Sci.* **2012**, *171*, 17.
[21] J. M. Gottfried, *Surf. Sci. Rep.* **2015**, *70*, 259.
[22] G. Bussetti, M. Campione, M. Riva, A. Picone, L. Raimondo, L. Ferraro, C. Hogan, M. Palummo, A. Brambilla, M.

Finazzi, L. Duò, A. Sassella, F. Ciccacci, *Adv. Funct. Mater.* **2014**, *24*, 958.
[23] B. Su, F. Li, R. Partovi-Nia, C. Gros, J.-M. Barbe, Z. Samec, H. H. Girault, *Chem. Commun.* **2008**, *40*, 5037.
[24] D. Kiessling, R. D. Costa, G. Katsukis, J. Malig, F. Lodermeyer, S. Feihl, A. Roth, L. Wibmer, M. Kehrer, M. Volland, P. Wagner, G. G. Wallace, D. L. Officer, D. M. Guldi, *Chem. Sci.* **2013**, *4*, 3085.
[25] C. J. Kaminsky, J. Wright, Y. Surendranath, *ACS Catal.* **2019**, *9*, 4, 3667.
[26] J. Ghilane, P. Hapiot, A. J. Bard, *Anal. Chem.* **2006**, *78*, 6868.
[27] A. Calloni, A. Abate, G. Bussetti, G. Berti, R. Yivlialin, F. Ciccacci, L. Duo, *J. Phys. Chem. C* **2015**, *119*, 21329.
[28] G. Berti, A. Calloni, A. Brambilla, G. Bussetti, L. Duo, F. Ciccacci, *Rev. Sci. Instrum.* **2014**, *85*, 073901.
[29] S. De Rosa, P. Branchini, R. Yivlialin, L. Duò, G. Bussetti, L. Tortora, *ACS Appl. Nano Mater.* **2020**, *3*, 691.
[30] G. Bussetti, R. Yivlialin, D. Alliata, A. Li Bassi, C. Castiglioni, M. Tommasini, C. S. Casari, M. Passoni, P. Biagioni, F. Ciccacci, L. Duò, *J. Phys. Chem. C* **2016**, *120*, 6088.
[31] C. Filoni, L. Duò, A. Li Bassi, A. Bossi, M. Campione, G. Capitani, I. Denti, M. Tommasini, C. Castiglioni, S. De Rosa, L. Tortora, G. Bussetti, *ChemNanoMat* **2020**, *6*, 567.
[32] G. Bussetti et al., submitted to ChemistryOpen. The dissolution mechanism of porphyrin nanocrystals is beyond the target of the present work, which is focused on the stability of the 2D film.
[33] F. Guo, Y. Wu, H. Chen, Y. Liu, L. Yang, X. Ai, X. Zou, *Energy Environ. Sci.* 2019,12, 684.
[34] R. Putra, H. Horino, I. I. Rzeznicka, *Catalysts* **2020**, *10*, 233.
[35] J. C. Manton, D. Hidalgo, L. Frayne, M. P. Brandon, J. G. Vos, M. T. Pryce, *Int. J. Hydrogen Energy* **2018**, *43*, 18843.
[36] C. J. Kaminsky, J. Wright, Y. Surendranath, *ACS Catal.* **2019**, *9*, 3667.
[37] D. Hötger, M. Etzkorn, C. Morchutt, B. Wurster, J. Dreiser, S. Stepanow, D. Grumelli, R. Gutzler, K. Kern, *Phys. Chem. Chem. Phys.* **2019**, *21*, 2587.
[38] J. H. Zagal, S. Griveau, K. I. Ozoemena, T. Nyokong, F. Bedioui, J. Nanosci, *Nanotechnology* **2009**, *9*, 2201.

Received: December 9, 2021
Accepted: September 30, 2021
Published online on January 22, 2022

Correction added on May 17, 2022 after first online publication: Cause: Funder statement has been added

